Mon. Not. R. astr. Soc. (1990) **243**, 620–628

Disentangling age and metallicity effects in the blueish nuclear population of M33, NGC 278 and NGC 404★

Alex A. Schmidt,[1,2] Eduardo Bica[3] and Danielle Alloin[4]

[1] *Universidade Federal de Santa Maria, Departamento de Matematica/NEPAE, Faixa de Camobi, Km 5, 97100 Santa Maria – RS – Brazil*
[2] *Astronomy Centre, University of Sussex, Falmer, Brighton BN1 9QH*
[3] *Universidade Federal do Rio Grande do Sul, Departamento de Astronomia, Av. Bento Gonçalves, 9500, 91500 Porto Alegre – RS – Brazil*
[4] *Observatoire de Paris, Section de Meudon, Département d'Astrophysique Extragalactique et de Cosmologie, F-92195 Meudon Cédex, France*

Accepted 1989 October 23. Received 1989 October 18; in original form 1989 May 2

SUMMARY

In this study, we have applied to the blueish nuclei of the spiral galaxies M33 and NGC 278 and to the dwarf lenticular NGC 404, a population synthesis method relying upon a base of star clusters, over the range 3700–9700 Å. We make use of a grid of star cluster spectral features as a function of age and metallicity. Whenever necessary, we refine this first approach by using the entire spectrum points directly. The algorithms employed are, in the first case a multiple minimization procedure with a statistical treatment of the acceptable solutions, and, in the second case a classical minimization procedure.

The near-infrared spectrum of the nucleus in M33 is very different from that of a metal poor globular cluster. Our synthesis indicates that the early type spectrum in the blue arises from young components and that the old, very metal-poor contributions at $[Z/Z_\odot] \leq -1.5$ are negligible in this object. The old component with metallicity in the range $-1.0 \leq [Z/Z_\odot] \leq -0.5$, as well as the intermediate age component, are important. The metallicity of the stellar population in the nucleus, at most, has reached up to the solar value.

The nucleus in NGC 278 is dominated by young components, at $t \leq 5 \times 10^8$ yr. The emission-line spectrum suggests that the star formation process is still operating. As for M33, the maximum metallicity in the nucleus is, at most, solar.

In NGC 404 the old population with $[Z/Z_\odot] \approx -0.5$ is dominant in the nucleus. The young component is weaker than in M33 and in NGC 278.

1 INTRODUCTION

The Local Group Sc galaxy M33 is rather intrinsically faint, with $M_B = -19.07$ (Sandage & Tammann 1981). Its proximity allows us to observe a small compact nucleus ≈ 6 parsec in diameter, with $M_v = -10.1$, which is comparable to the largest globular clusters (O'Connell 1983). The stellar content of the semi-stellar nucleus (SSN) of M33 has been for some time a matter of debate. McClure, Cowley & Crampton (1980) interpreted the spectral features in the range 3900–4200 Å as being from an old metal-poor population, similar to a metal-poor globular cluster. However, more recent analyses, based on spectral synthesis models, tend to indicate rather that the early-type spectral characteristics in the blue arise from young stars in a composite age population (Cowley, Crampton & McClure 1982; O'Connell 1983). As well, both a population synthesis over the range 1200–3000 Å, in conjunction with *UBV* colours (Ciani, D'Odorico & Benvenuti 1984), and an analysis of optical and infrared data (Gallagher, Goad & Mould 1982) support a mixture of young and old components in this object.

NGC 404 is a dwarf lenticular with $M_B = -17.37$ at the edge of the Local Group and NGC 278 is an Sbc galaxy with $M_B = -20.5$ (Sandage & Tammann 1981). NGC 278 exhibits a peculiar spiral structure with a high surface brightness in the inner arm regions (de Vaucouleurs & de Vaucouleurs 1964, and references therein). As far as we are aware, no detailed population syntheses have ever been published for these two galaxies. However, their emission-line spectra have been analysed by Stauffer (1982, 1983) and Keel (1983).

Recently a new population synthesis method, which uses a star cluster spectral library and a grid of the star cluster

★ Based upon data collected at the Observatoire de Haute Provence (CNRS).

spectral properties as a function of age and metallicity, has been developed (Bica & Alloin 1986a,b, 1987a). As, in this method, the IMF and the stellar evolution are implicit in the elements of the base, the synthesis problem is less parameter-dependent and considerably simplified. However, the age and metallicity values adopted for the star clusters, which we take from the literature, are indeed sensitive to the stellar formation and evolution theories. If these were modified, then our age and metallicity scales would change accordingly. But it is still a second order effect which does not affect our relative conclusions. The method has already been applied to a variety of nuclei to be found in Shapley–Ames galaxies and has provided valuable information on their age and metal content (Bica 1988).

In the present paper we apply this star cluster method to synthesize populations in the nuclei of M33, NGC 278 and NGC 404, which share the characteristics of an early-type spectrum. The grid of star cluster equivalent widths, W_λ [age, $(Z/Z_\odot)$], spans the full ranges in age and metallicity relevant to this problem. The method is thus particularly suitable for discriminating between the effects of young and old metal-poor populations: a quality especially required for a *quantitative* estimate of the proportions of various components in the composite stellar content of galaxy nuclei like M33.

In Section 2 we briefly present the observations and the reduction procedures. In Section 3 we recall some aspects of the synthesis method. In Sections 4, 5 and 6 we present the results for M33, NGC 278 and NGC 404, respectively. We discuss in Section 7 the population-subtracted emission component for each nucleus. Our concluding remarks are given in Section 8.

2 OBSERVATIONS AND REDUCTION PROCEDURES

We observed the galaxies in 1987 August, with the Carelec spectrograph at the Cassegrain focus of the 1.93-m telescope at the Haute Provence Observatory. An RCA CCD detector with 320 versus 512 pixel of 30-μm size was employed. The slit was 3.5 arcsec wide and 5.3 arcmin long, oriented along the East–West direction. The spectral ranges covered were 3500–7300 Å and 6200–10000 Å with a 150 gr mm^{-1} grating in the first order providing a dispersion of 260 Å mm^{-1}. Helium and Argon comparison lamps were used, respectively, for the visible and near-infrared ranges. The resolution measured as the FWHM of comparison lines was 18 Å. An internal tungsten filament lamp provided a flat-field frame after each object exposure. This procedure allows the interference fringes in the near-infrared frames to be eliminated by a simple flat-field division. Standard stars BD+28°4211, Hiltner 102 and G191B2B were used for flux calibrations (Oke 1974; Stone 1977). Typical exposures were of 5 min for the stars, 20–40 min for M33, 25–30 min for NGC 278 and 15–25 min for NGC 404.

The reductions were made with the IHAP and eVe software at the Institut d'Astrophysique de Paris and Observatoire de Paris/Meudon. The usual procedure for CCD reductions was followed: bias subtraction, flat-fielding correction, spectrum extraction, sky subtraction and wavelength and flux calibrations. The hot standard stars were used for correcting atmospheric molecular band absorptions as described in Bica & Alloin (1987a). The pixel rows for sky subtraction, on each side of the nucleus, were 0.62 arcmin $< r <$ 1.6 arcmin for M33, 0.73 arcmin $< r <$ 2.1 arcmin for NGC 278 and 1.2 arcmin $< r <$ 2.4 arcmin for NGC 404. The luminosity peak in the central 9 arcsec was considered to represent the M33 semi-stellar nucleus (SSN). For NGC 278 we have summed pixel rows in the central 16 arcsec while for NGC 404 the high surface brightness region extends within the inner 63 arcsec. Adopting the distance moduli from Sandage & Tammann (1981), the nuclear regions observed correspond to 13×37 pc for M33, 280×1300 pc for NGC 278 and 70×1280 pc for NGC 404. The 900 Å overlap of the spectra allowed an excellent merging of the two spectral ranges observed. Foreground reddening corrections from Burstein & Heiles (1984) were adopted: $E(B-V)_G=0.05$ for M33; $E(B-V)_G=0.18$ for NGC 278 and $E(B-V)_G=0.06$ for NGC 404.

We have measured the equivalent widths of strong features with continuum tracing criteria, as shown in Bica & Alloin (1988), and fixed window limits as defined in Bica & Alloin (1986a; 1987a). The measurements were carried out with a spectral analysis package developed in Porto Alegre. Results for W_λ, together with the continuum distribution corrected for the foreground reddening and normalized to 5870 Å, are given in Tables 1(a and b), respectively. These measurements can be compared with those from other galaxies that we have previously analysed, in particular other blue nuclei like NGC 5102 and NGC 5236 (Bica & Alloin 1987a,b).

3 THE SYNTHESIS METHOD

The algorithm we have used to perform the synthesis is that described in Schmidt, Bica & Dottori (1989). It consists of minimizing the differences between a set of observed and synthetic equivalent widths of spectral features. The synthetic features are obtained from a 35-component base, each component corresponding to a star cluster evolutionary stage at a particular metallicity. Each component in the age versus metallicity plane is represented by six metallic features and three Balmer lines, as well as their underlying continuum, from a grid of star cluster spectral properties in the visible and near-infrared ranges (Bica & Alloin 1986b, 1987a). In this procedure we do not make use of the full spectral information.

The minimization procedure must be carried out in the framework of a degenerate inverse problem with a non-unique solution. We transform the problem into a series of minimization tasks, each task having one of the 35 components fixed at a 10 per cent step contribution between 0 and 100 per cent. Every solution, which represents a local minimum around the fixed component, is subsequently tested against a set of windows of maximum allowed difference between the observed and synthetic features we use. Finally *we calculate an average solution from the local solutions satisfying all feature windows.* Each solution entered in the average determination not only stands for its contribution to a synthetic model, but also represents its probability of being present in any acceptable solution to the problem, using this base. A thorough discussion of this procedure is provided in Schmidt, Bica & Alloin (1990) with regard to the eventuality of finding non-unique solutions, as a result of intrinsic errors in the observable parameters to be fitted. The

Table 1.(a) Measured equivalent widths (Å) for the galaxy nuclei; (b) continuum points F_λ relative to F_λ(5870 Å) corrected for the foreground reddening (Section 2).

(a)

Window #	Feature Identifications	Limits (Å)	M33	NGC278	NGC404
2	CN+H9	3814-3862	7.3	7.0	8.5
3	CN+H8	3862-3908	7.0	6.6	6.9
4	CaII K	3908-3952	6.3	5.7	8.8
5	CaII H+Hε	3952-3988	9.2	9.5	9.6
9	Hδ	4082-4124	6.9	7.8	5.2
10	FeI	4124-4150	1.7	1.4	1.4
11	CN	4150-4214	1.6	1.4	2.6
12	CaI	4214-4244	0.7	0.6	1.2
13	FeI	4244-4284	1.8	1.0	2.7
14	CH G	4284-4318	3.9	3.3	5.1
15	Hγ	4318-4364	6.8	6.7	5.1
16	FeI	4364-4420	3.3	2.8	3.6
27	Hβ	4846-4884	6.1	4.3	4.5
31	FeI	4998-5064	2.5	2.6	2.1
32	FeI, C_2	5064-5130	2.0	2.0	2.7
33	MgH, C_2	5130-5156	1.1	1.4	1.6
34	MgI, MgH	5156-5196	3.4	3.5	4.5
35	MgH	5196-5244	2.3	2.7	3.0
36	FeI	5244-5314	2.6	3.0	3.2
48	NaI	5880-5914	2.5	3.0	2.5
54/5/6/7	TiO	6156-6386	10.8	11.4	12.2
59	CaI, FeI	6474-6540	1.3	1.5	1.3
60	Hα	6540-6586	2.8	-20.0	-5.1
62	TiO, [SII]	6670-6736	0.9	-2.8	-3.7
66/7/8	TiO	7050-7464	20.0	18.4	17.6
71	TiO	7704-7852	5.2	5.4	5.3
72	CN	7852-8040	7.4	13.0	12.7
74	NaI, TiO?	8160-8234	0.8	1.3	1.5
75/6	TiO, TiI	8234-8476	10.5	10.1	9.1
77	CaII, TiO	8476-8520	3.5	3.4	4.4
78	CaII, TiO	8520-8564	5.2	5.4	5.6
79	P14, TiO	8564-8640	2.1	3.4	3.5
80	CaII, TiO	8640-8700	4.6	5.3	5.2
81	P12, FeI	8700-8786	2.5	1.7	2.0
83/4	TiO, P11+10	8844-9066	7.8	7.6	5.0

(b)

λ(Å)	M33	NGC 278	NGC 404
4020	0.99	1.23	0.75
4570	1.04	1.17	0.91
5340	1.02	1.05	0.97
6630	0.91	0.86	0.94
6990	0.88	0.82	0.92
7520	0.86	0.78	0.92
8040	0.81	0.72	0.87
8408	0.76	0.68	0.85
8700	0.74	0.67	0.84
9100	0.72	0.65	0.82

statistical approach we use here keeps this eventuality at a very low level. On the other hand, we are presently testing our algorithms – direct combinations and multi-minimization tasks – against combinations of the star cluster base elements, built *a priori* and then blindly analysed: the original combination is always found within a 10 per cent scatter.

This method allows one to sweep the vector space generated by the 35-component base in a fast and efficient way, yielding a representative set of acceptable solutions to the synthesis problem. The code was written in FORTRAN 77 and linked to the MINOS 5 optimization system (Murtagh & Saunders 1987). The computations were carried out in the COBRA 1400 (Eclipse 8000 II) computer of the Instituto de Fisica – UFRGS, Porto Alegre. The typical CPU time for each object was 20 min.

Following Schmidt *et al.* (1989) the computations were performed in two ways: first we covered the whole age versus metallicity plane and, secondly, we restricted the solution to chemical evolutionary paths through the plane (Bica 1988). These evolutionary paths can be of two types: for type A, the maximum metallicity is attained within the old-age bin, while for type B an additional metallicity increase may occur between the old-age bin and the bin at 5×10^9 yr. The results are expressed in terms of the flux contributions, at 5870 Å, from the various components; we also provide the number of acceptable solutions found, the observed W_λ, the residuals ($W_{\lambda\mathrm{obs}}-W_{\lambda\mathrm{synt.}}$) and the feature windows, and finally the corresponding reduced chi-squared (χ^2) of the solution.

4 STELLAR POPULATION SYNTHESIS OF THE NUCLEUS IN M33

We provide in Fig. 1 a direct comparison of the spectra from the M33 semi-stellar nucleus (SSN) corrected for the foreground reddening $E(B-V)_G=0.05$ and from the star cluster group G5 (Bica 1988), which consists of an average of reddening corrected globular clusters with $[Z/Z_\odot]\approx-2$, like M15 (NGC 7078) and M53 (NGC 5024). As already pointed out by O'Connell (1983) and Gallagher *et al.* (1982) there is a qualitative similarity of spectral features in the blue part of the spectrum between the nucleus of M33 and metal-poor globular clusters. However, quantitative measurements reveal that the equivalent widths of Balmer lines and Mg I are stronger in M33 while the *K* line of Ca II is weaker. Fig. 1 shows even more striking feature strength differences in the near-infrared region. Indeed, molecular bands like TiO are quite strong in M33, resembling metal-rich populations, while they are absent in the metal-poor globular clusters. Also, the Ca II triplet is much stronger in M33. This simple comparison definitely rules out the possibility that the nucleus of M33 is dominated by a very metal-poor old population. In fact the progressive dilution of metallic

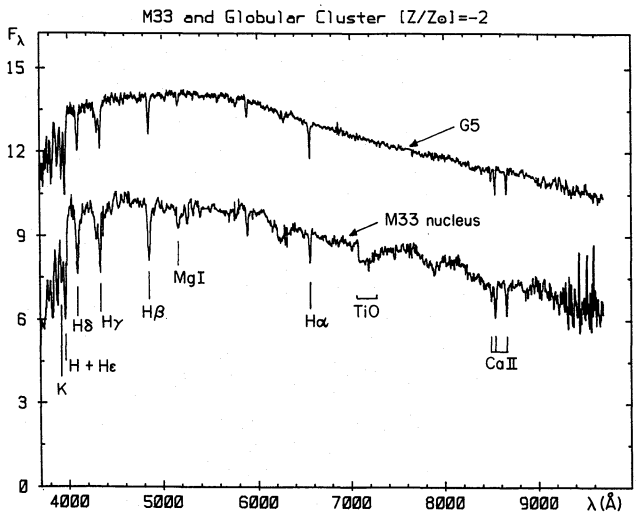

Figure 1. Comparison of the nucleus of M33 with an average of globular clusters at $[Z/Z_\odot]\approx-2$. The globular cluster spectrum has been shifted along the intensity scale for clarity. Both spectra are normalized to $F_\lambda=10$ at 5870 Å. Notice the strong metallic features in the near-infrared spectrum of M33.

features towards the blue is, rather, a characteristic property of young star clusters (Bica & Alloin 1986a, 1988). Fig. 1 also shows that M33 and the metal-poor globular clusters, which differ significantly in line strength, also present similar spectral energy distributions. The line strength differences would remain undetected in broad-band colours over this range. *This example evinces the major importance of analysing spectral features, and not only broad-band colours, for accurate population synthesis.*

We show in Table 2(a) the whole-plane solution for the M33 SSN. Similar to the blue nucleus of NGC 5102, the contributions tend to scatter through the plane (Schmidt *et al.* 1989a), certainly because additional information at shorter wavelengths is necessary for sorting out a better focused solution. However, the whole-plane solution suggests that the old and intermediate-age components are slightly metal deficient with respect to the Sun. It also indicates that the young components ($t \leq 5 \times 10^8$ yr) provide an important contribution to the flux. The best χ^2 for solutions along a chemical evolutionary path is found for a maximum metallicity $[Z/Z_\odot] = -0.5$ (Tables 2b and c) with no significant difference between path types A or B. However, it is interesting to look at the redistribution of flux fractions in the absence of the old-age component at $[Z/Z_\odot] = -0.5$ for path $B[-0.5]$ (Table 2c). The path solutions which attain solar metallicity (path A[0.0] not shown and B[0.0] in Table 2d) present larger χ^2. With respect to the syntheses reaching $[Z/Z_\odot] = -0.5$ only, the contributions to the old-age bins are stronger. The large-metallicity paths have larger χ^2 and provide very complex contributions in the old-age bin suggesting mathematical internal compensations between metal-rich and metal-poor components to reproduce the W_λ of the M33 nucleus. They should be discarded.

So far we have used only the equivalent widths W_λ from the grid star cluster spectral properties. The continuum distribution has not had much weight in our computations as the synthetic W_λ depends only at second order on the underlying continua of the lines. We then performed an additional synthesis for M33 using the point by point spectrum in the range 3700–9700 Å with a 2 Å step. The input base, in this case, consists of the star cluster spectral groups defined in Bica (1988). The metallicity of the young (Y1 to Y4) and intermediate (I1 and I2) age groups are particularly suitable for a direct synthesis of the M33 SSN because they contain LMC and galactic disc clusters. The average metallicity $[Z/Z_\odot]$ of the galactic globular cluster groups G2 and G5 ranges from -0.4 to -2. The very strong-lined group G1, with globular clusters like NGC 6528, is not of interest for the M33 SSN according to results in Tables 2(b–d). We have added to our base an H II region continuum, free of emission lines, derived from observed H II regions affected by internal reddening: it acts as a diluter of blue spectral features in the synthesis. For the population synthesis we have excluded the Hα region 6520–6600 Å owing to the possibility of emission at a low level. As well we have excluded the spectral regions in which residues of atmospheric molecular band corrections might occur: 6830–6940, 7550–7620 and 9280–9700 Å. Combinations of the 11-base components, together with the internal reddening $E(B-V)_i$, were optimized with the MINOS system, minimizing the differences between the complete observed spectrum of the M33 nucleus [corrected for the foreground reddening $E(B-V)_G = 0.05$] and the synthetic one. This synthesis was meant to provide an improvement of the grid calculations for the paths A[−0.5] and B[0.0]. Therefore, the component contributions were allowed to vary between their corresponding flux fractions from Tables 2(b and d). The results are shown in Table 3. An

Table 2. Percentage flux fractions at 5870 Å from each component in the metallicity versus age plane, for the nucleus in M33; (a) the whole-plane solution; (b) the path solution of type A, reaching a maximum metallicity $[Z/Z_\odot] = -0.5$, labelled A[−0.5]; (c) the path solution of type B, reaching a maximum metallicity $[Z/Z_\odot] = -0.5$, labelled B[−0.5]; (d) the path solution B[0,0] and (e) achievements of the various models.

a)

RHII	E7	5E7	E8	5E8	E9	5E9	> E10	Age $[Z/Z_\odot]$
4.1	14.1	1.1	1.7	0.9	0.6	0.6	1.3	+ 0.6
	0.7	1.1	0.8	1.1	0.5	0.6	0.8	+ 0.3
	0.5	1.1	0.8	1.9	0.8	0.8	0.8	0.0
	2.1	1.5	5.3	23.5	2.5	11.0	1.1	- 0.5
					1.6	10.4	1.1	- 1.0
						0.9	0.8	- 1.5
							1.0	-2.0

Acceptable solutions : 185 ; $\chi^2 = 0.480$

b)

RHII	E7	5E7	E8	5E8	E9	5E9	> E10	Age $[Z/Z_\odot]$
1.5								+ 0.6
								+ 0.3
								0.0
	19.4	4.3	9.1	22.3	8.3	28.0	5.2	- 0.5
							1.2	- 1.0
							0.6	- 1.5
							0.2	- 2.0

Acceptable solutions : 49 ; $\chi^2 = 0.478$

c)

RHI	E7	5E7	E8	5E8	E9	5E9	> E10	Age $[Z/Z]_\odot$
1.7								+ 0.6
								+ 0.3
								0.0
	19.5	4.9	8.4	22.0	10.0	20.8		- 0.5
							1.8	- 1.0
							0.7	- 1.5
							0.2	- 2.0

Acceptable solutions : 43 ; $\chi^2 = 0.481$

d)

RHII	E7	5E7	E8	5E8	E9	5E9	> E10	Age $[Z/Z]_\odot$
2.7								+ 0.6
								+ 0.3
	13.6	4.8	24.0	7.7	5.1	3.4		0.0
							15.7	- 0.5
							18.4	- 1.0
							2.0	- 1.5
							2.5	- 2.0

Acceptable solutions : 54 ; $\chi^2 = 0.696$

e)

Features	Observed W_λ (Å)	Window (Å)	Residue (Å) a	b	c	d
CaII K	6.3	2.5	0.2	0.0	0.0	0.4
CN 4216	1.6	3.0	- 1.4	- 1.3	- 1.3	- 1.8
CH G	3.9	1.5	0.9	0.7	0.7	1.0
MgI + MgH	3.4	1.8	0.0	0.1	0.2	0.0
CaII 8542	5.2	1.2	0.5	0.8	0.8	0.6
CaII 8662	4.6	1.2	0.2	0.5	0.5	0.4
Hδ	6.9	2.5	- 0.7	- 0.7	- 0.7	- 0.5
Hγ	6.8	2.0	0.4	0.4	0.4	0.2
Hβ	6.1	1.2	0.3	0.3	0.3	0.6

Table 3. Synthesis using the integrated spectra of star cluster groups directly as a base, in the case of the nucleus in M33.

Cluster Group	Age(yr)	[Z/Z⊙]	M33 (% flux)	NGC 404 (% flux)
HII	$< 5 \times 10^6$	0.0 to -0.5	1.5	1.7
Y1	10^7	-0.3	13.6	14.2
Y2	5×10^7	-0.2 to -0.6	4.3	2.3
Y3	10^8	+0.1 to -1.0	9.1	1.6
Y4	5×10^8	-1.1	7.7	4.4
I1	10^9	0.0	8.3	3.8
I2	5×10^9	-0.6 to -1.0	24.0	13.7
G1	$> 10^{10}$	+0.2 to 0.0	0.0	0.0
G2	$> 10^{10}$	-0.4	15.7	46.0
G3	$> 10^{10}$	-1.0	15.0	11.9
G4	$> 10^{10}$	-1.5	0.6	0.2
G5	$> 10^{10}$	-2.0	0.2	0.2

Columns: (1) identification of the star cluster group according to Bica (1988); (2) and (3) age and metallicity of the mean star cluster in each group; (4) and (5) synthesis results for the nucleus of M33 and NGC 404 expressed as the flux fractions at 5870 Å. The internal reddening was a free parameter in the optimization; it came out as $E(B-V)_i = 0.05$ and 0.07 for M33 and NGC 404, respectively.

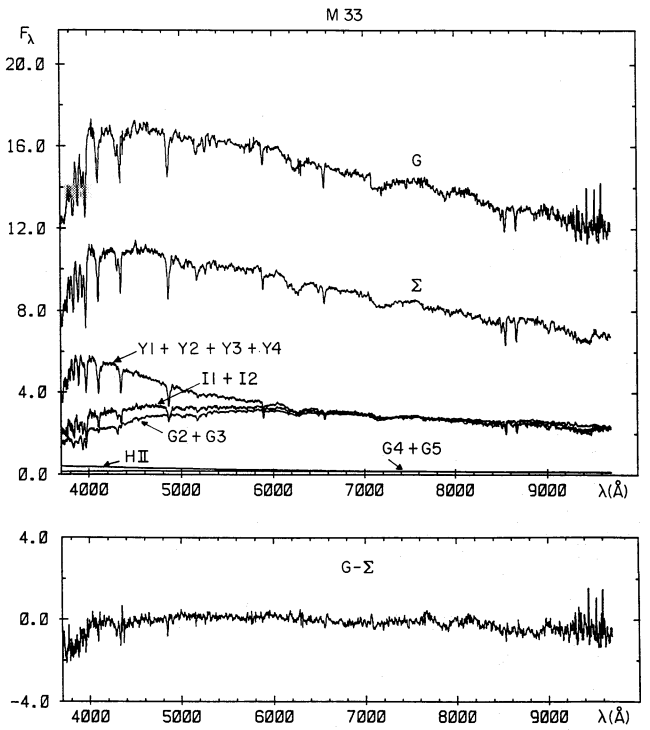

Figure 2. Visualization of the synthesis solution for the nucleus in M33 from Table 3. The upper spectrum is that of the galaxy nucleus (G) corrected for the foreground reddening $E(B-V)_G = 0.05$, and an internal reddening $E(B-V)_i = 0.05$ derived through the synthesis in Table 3. Both the synthetic spectrum (Σ) and the components are shown. The young component is important while the old very metal-poor one with $[Z/Z_\odot] \leq -1$ is negligible. The difference spectrum is shown in the lower part of the figure.

internal reddening $E(B-V)_i = 0.05$ was derived. The solution is illustrated in Fig. 2.

In conclusion, all solutions indicate that the young components ($t \leq 5 \times 10^8$ yr) are important in the M33 SSN, in particular in the blue where they predominantly contribute to the light, and that the old very metal-poor components, $[Z/Z_\odot] \leq -1.5$, are negligible. The relative importance of the intermediate age component and of the old moderately metal-rich one remains to be determined with more precision. This will be possibly achieved using observations which cover a spectral range extending to the ultraviolet.

5 STELLAR POPULATION ANALYSIS IN NGC 278

We show in Table 4(a) the whole-plane solution for NGC 278. As already pointed out in the discussion about M33

Table 4. Percentage flux fractions at 5870 Å, from each component in the metallicity versus age plane, for the nucleus in NGC 278; (a) the whole-plane solution; (b) the path solution of type A, reaching a maximum metallicity $[Z/Z_\odot] = -0.5$, labelled A[−0.5]; (c) the path solution of type B, reaching a solar metallicity, labelled B[0.0] and (d) achievements of the various models.

a)

RHII	E7	5E7	E8	5E8	E9	5E9	< E10	Age [Z/Z⊙]
1.9	17.1	1.8	3.3	1.1	0.5	1.0	2.6	+ 0.6
	0.9	1.8	1.5	1.0	0.5	0.6	0.7	+0.3
	0.7	1.8	1.4	1.4	0.7	0.5	0.7	0.0
	5.0	1.8	5.9	26.5	1.8	7.3	1.6	- 0.5
					2.1	1.1	1.6	- 1.0
						0.7	0.7	- 1.5
							0.5	- 2.0

Acceptable solutions : 205 ; $\chi^2 = 0.429$

b)

RHII	E7	5E7	E8	5E8	E9	5E9	< E10	Age [Z/Z⊙]
0.9								+ 0.6
								+ 0.3
								0.0
	19.9	6.2	10.1	28.0	7.3	8.1	17.8	- 0.5
							1.1	- 1.0
							0.5	- 1.5
							0.2	- 2.0

Acceptable solutions : 56 ; $\chi^2 = 0.576$

c)

RHII	E7	5E7	E8	5E8	E9	5E9	< E10	Age [Z/Z⊙]
1.5								+ 0.6
								+ 0.3
	15.1	21.7	19.5	7.3	2.8	4.9		0.0
							18.6	- 0.5
							5.7	- 1.0
							1.8	- 1.5
							1.2	- 2.0

Acceptable solutions : 57 ; $\chi^2 = 0.737$

d)

Features	Observed W_λ (Å)	Window (Å)	Residue (Å) a	b	c
CaII K	5.7	2.5	0.2	- 0.1	0.4
CN 4216	1.4	3.0	-1.4	-1.1	-1.8
CH G	3.3	1.5	0.7	0.4	0.9
MgI + MgH	3.5	1.8	0.1	0.4	0.2
CaII 8542	5.4	1.5	0.3	1.0	0.5
CaII 8662	5.3	1.5	0.6	1.2	0.8
Hδ	7.8	2.5	-0.2	-0.2	0.1
Hγ	6.7	2.0	0.1	0.1	-0.1

(Section 4) and about other blue nuclei (Schmidt *et al.* 1989) there is a large scatter of the components through the plane. But again the solution suggests that young components are dominant and that the old component is metal deficient. The best χ^2 for solutions along chemical evolutionary paths occurs for model A[−0.5] which is given in Table 4(b). As a comparison we also provide in Table 4(c), the best solution in the case of a solar metallicity path B[0.0]: it exhibits, with respect to the former, a transfer of the intermediate age components towards younger components ($t \leq 5 \times 10^8$ yr) as well as a rearrangement of the young component contributions themselves. However, the global results are similar. We display in Fig. 3 the solution corresponding to the chemical evolutionary path A[−0.5]. The resulting internal reddening is null which is not unexpected for a face-on galaxy. The young component is dominant and the old very metal-poor one is negligible. The intermediate age and the old $[Z/Z_\odot] = -0.5$ components are of comparable importance. The difference spectrum (G − Σ) given in the lower part isolates the emission-line spectrum from ionized gas, which is discussed in Section 7. Both the blue stellar components, stronger than in the M33 nucleus, and the presence of strong emission lines demonstrate that the burst of star formation in NGC 278 is still operating. The solutions along the chemical evolutionary paths indicate that the maximum metallicity attained in this object is at most solar: it is probably somewhat metal deficient.

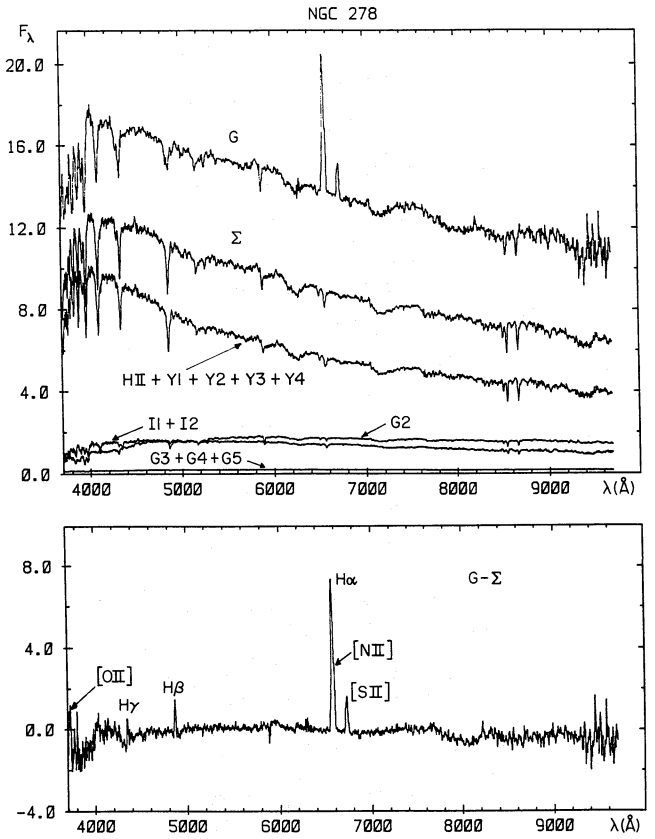

Figure 3. Visualization of the synthesis results for the nuclear region in NGC 278 from Table 4(b). The real galaxy spectrum (G) has been corrected for the foreground reddening $E(B-V)_G = 0.18$ and no further internal reddening was necessary during the stellar population synthesis. In the synthetic spectrum (Σ) the young component dominates. In the difference spectrum (lower part) we obtain the emission line spectrum from the ionized gas.

Although NGC 278 is intrinsically quite bright $M_B = -20.5$ (Section 1), there is evidence that it is not a very massive galaxy. We have verified that the pixel rows external to the nuclear region in our data indicate the presence of central arms with high surface brightness and a spectrum even bluer than that of the nuclear region. An intense star formation extending from the nucleus to the inner arms is certainly responsible for the high luminosity of this galaxy, which in a quiescent epoch may be a small spiral like M33 ($M_B = -19.07$).

6 SYNTHESIS OF THE STELLAR POPULATION IN NGC 404

We provide similarly for NGC 404 the various solutions in Table 5. Regarding the whole age versus metallicity plane

Table 5. Percentage flux fractions at 5870 Å, from each component in NGC 404, for various population syntheses; (a) the whole plane solution; (b) the path solution of type A, reaching a metallicity $[Z/Z_\odot] = -0.5$; (c) the path solution of type B, up to a solar metallicity; (d) achievements of the various models.

a)

RHII	E7	5E7	E8	5E8	E9	5E9	<E10	Age [Z/Z⊙]
3.9	13.3	0.6	0.3	1.2	0.8	2.2	4.0	+ 0.6
	0.4	0.6	0.3	1.2	0.9	1.0	0.9	+ 0.3
	0.6	0.6	0.3	1.2	1.2	1.2	1.2	0.0
	0.9	0.6	0.4	7.3	2.1	14.6	21.3	- 0.5
					1.2	2.0	7.9	-1.0
						0.9	1.2	-1.5
							1.9	-2.0

Acceptable solutions : 175 ; $\chi^2 = 1.043$

b)

RHII	E7	5E7	E8	5E8	E9	5E9	<E10	Age [Z/Z⊙]
1.7								+ 0.6
								+ 0.3
								0.0
	14.2	2.4	1.6	8.5	3.8	19.8	46.0	-0.5
							1.5	- 1.0
							0.2	- 1.5
							0.2	- 2.0

Acceptable solutions : 41 ; $\chi^2 = 0.974$

c)

RHII	E7	5E7	E8	5E8	E9	5E9	<E10	Age [Z/Z⊙]
4.2								+ 0.6
								+ 0.3
	14.6	2.3	4.5	4.4	8.8	9.2		0.0
							38.9	- 0.5
							11.9	- 1.0
							0.6	- 1.5
							0.5	- 2.0

Acceptable solutions : 48 ; $\chi^2 = 1.221$

d)

Features	Observed W_λ (Å)	Window (Å)	Residue (Å) a	b	c
CaII K	8.8	2.5	0.9	0.6	1.0
CN 4216	2.6	3.0	- 2.0	- 1.7	- 2.2
CH G	5.1	1.5	0.8	0.6	0.8
MgI + MgH	4.5	1.8	0.2	0.4	0.3
CaII 8542	5.6	1.5	0.8	1.2	1.0
CaII 8662	5.2	1.5	0.8	1.1	0.9
Hδ	5.2	2.5	- 0.7	- 0.6	- 0.4
Hγ	5.1	2.0	- 0.2	- 0.2	- 0.1

solution (Table 5a), we find that the old population is more important than in the case of previously analysed nuclei. This solution suggests that NGC 404 is metal deficient. The best χ^2 is obtained for the chemical evolutionary path A[−0.5] shown in Table 5(b). For comparison we give in Table 5(c) the path solution B[0.0] which reaches a solar metallicity. The basic change in the latter is a vanishing of the intermediate age component with respect to the A[−0.5] path. As in the case of M33, it is worth improving the synthesis by a direct use of the spectra of the cluster groups. The component contributions were allowed to vary between the values obtained in solutions A[−0.5] and B[0.0]. The results are shown in column 5 of Table 3 and the spectra are visualized in Fig. 4. The resulting internal reddening is found to be $E(B-V)_i=0.07$. The young component contribution is weaker than in M33 or NGC 278 nuclei but is more important than in most nuclei synthesized in Bica (1988). The old population with $[Z/Z_\odot]=-0.5$ is dominant. The intermediate age component is also important with a 17 per cent fraction of the optical flux at 5870 Å. The emission-line component has been isolated in the (G−Σ) difference and its characteristics are discussed in Section 7.

7 ANALYSIS OF THE STELLAR-FREE EMISSION COMPONENTS

The stellar subtracted spectra [residuals (G−Σ)] are used to search for emission lines. Spectral regions where strong emission lines occur are shown in detail in Fig. 5(a and b), respectively for Hα, [N II] 6584 Å, [S II] 6717, 6731 Å, and Hβ, [O III] 4959, 5007 Å. In the case of the M33 SSN, [N II] 6584 Å is present with $W_e=0.6$ Å, taking into account the stellar population continuum level in this region. It has also been detected at higher resolution by Rubin & Ford (1986). NGC 278 and NGC 404 present strong emission lines which we have measured through Gaussian fits as in Bonatto, Bica & Alloin (1989). This procedure allows a straightforward deblending of Hα and [N II]. The intensities, with respect to Hα, are shown in Table 6 together with previous results for NGC 278 (Stauffer 1983) and NGC 404 (Stauffer 1982; Keel 1983). At this stage our spectra are corrected for the foreground reddening and the internal reddening in the central regions which affects the stellar populations (see previous sections). Therefore, we have also applied these

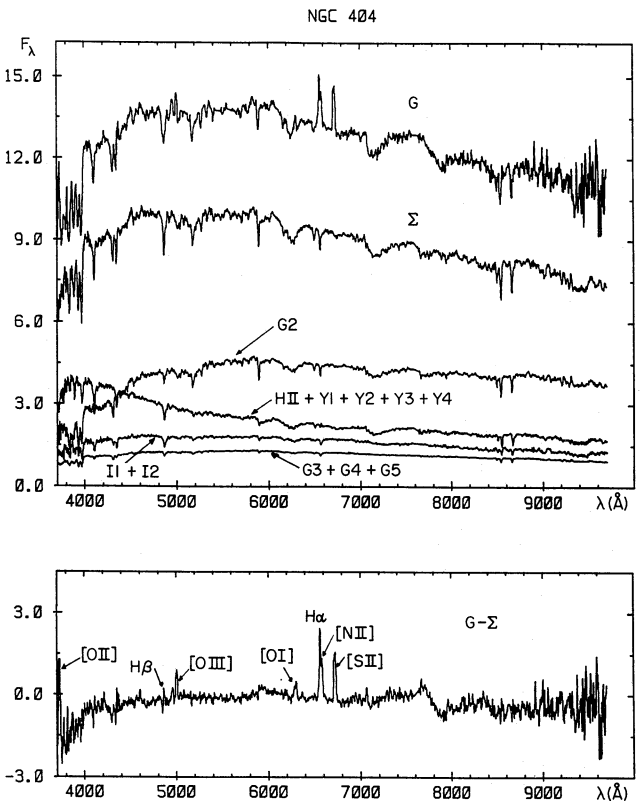

Figure 4. Visualization of the synthesis results for NGC 404, from Table 3. The observed galaxy spectrum has been corrected for the foreground reddening $E(B-V)_G=0.06$ and an internal reddening $E(B-V)_i=0.07$, derived through the synthesis (Table 3). In the synthetic spectrum (Σ) the old population with $[Z/Z_\odot]=-0.5$ dominates the light, but the young population is also important. The emission line spectrum appears in the (G−Σ) difference, in the lower part of the figure.

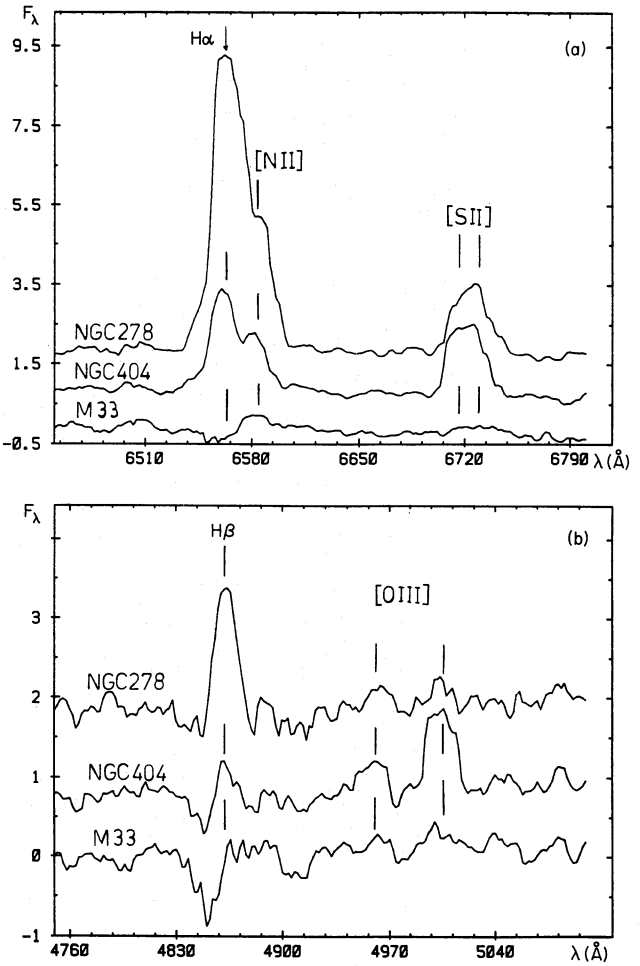

Figure 5. (a and b) Zoom on the emission lines in the (observed minus synthetic) spectra. The vertical scale corresponds to a continuum value $F_\lambda=10$ at 5870 Å, in the spectra including the stellar population. Discussion in Section 7.

Table 6. Emission line intensities with respect to Hα (normalized at 100).

Line λ (Å) identification	NGC 278 this paper	NGC 278 Stauffer (1983)	NGC 404 this paper	NGC 404 Stauffer (1983)	NGC 404 Keel (1983)
[OII] 3727	42.2		145.5		
Hγ 4340	13.5:				
Hβ 4861	16.9		15.3	0.0	29.1
[OIII] 4959	2.6		15.6		
[OIII] 5007	3.2		48.3	36.3	51.2
[OI] 6300	3.0		16.9	30.3	17.6
[OI] 6364			6.3		
Hα 6563	100.0	100.0	100.0	100.0	100.0
[NII] 6584	27.2	45.6	54.1	46.4	57.3
[SII] 6717, 31	30.9	35.9	96.5	82.2	114.2
[SIII] 9069	< 4.5		< 25.2		
[SIII] 9532	< 23.2		< 57.6		

(i) The ratio [N II] λ6584/λ6548 = 3 was imposed in the deblending from Hα; (ii) all values including Keel's and Stauffer's have been corrected for the foreground reddening and for the internal reddening associated with the stellar population, according to the present paper. Reddening associated with the line-emitting regions themselves is discussed in Section 7, and has been left in the present figures.

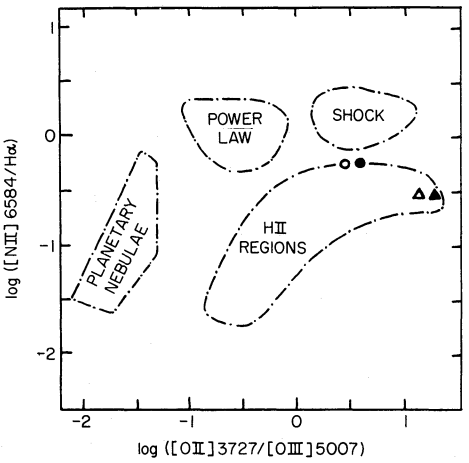

Figure 6. Logarithmic plot of the line intensity ratios [N II] λ6584/Hα versus [O II] λ3727/[O III] λ5007. We have enclosed the regions containing most of BPT's objects. Triangles refer to NGC 278 and circles refer to NGC 404. Open symbols correspond to data corrected for the foreground reddening and the internal reddening associated with the stellar populations. Black symbols represent data points with an additional reddening correction intrinsic to the line emitting regions.

reddenings to the data produced from other studies in Table 6. Stauffer's [N II]/Hα for NGC 278 is stronger than ours, which could be explained by his underestimation of the stellar absorption Hα feature. In fact, in one of the two procedures which he used, he did not correct for any underlying stellar population. In the case of NGC 404, Keel's results resemble ours; all three works agree within 10–15 per cent, except for the Hβ line. Stauffer has used a red galaxy template population for the underlying population of NGC 404: for such a blueish nucleus this underestimates Hβ in absorption and consequently the Hβ emission is underestimated in the difference spectrum by Stauffer. On the other hand, Keel's value is larger than ours which is due, we think, to an excess of blue stellar content in his population model based upon stellar spectra. We point out that in our study we use a wider spectral range, including Ca II triplet, which is essential to constrain better the stellar population synthesis. We conclude, by means of this comparison, that our procedure results in a precision better than 15 per cent, although the uncertainty may be larger for critical cases like Balmer lines and very weak lines like [O III] 4959, 5007 Å in NGC 278, which are not found within the expected ratio 1:3.

Comparing the Hα emission-line intensity to the continuum intensity near Hα, we obtain $W_e(H\alpha) = 17.9$ and 4.9 A, respectively for NGC 278 and NGC 404. The reddening associated with the line-emitting regions themselves, $E(B-V)_E$, can then be derived from Hα/Hβ in Table 6. For NGC 278, we obtain Hα/Hβ = 5.9 and for NGC 404, Hα/Hβ = 6.5, implying a reddening intrinsic to the emitting regions of $E(B-V)_E = 0.66$ and 0.75, respectively. A large uncertainty on the Balmer line ratio is indeed critical: for comparison, Keel's results in the case of NGC 404 lead to $E(B-V)_E = 0.28$.

Following Baldwin, Phillips & Terlevich (1981, hereafter BPT) we have attempted to identify the excitation mechanism in these nuclei, using line ratios in the visible region (Fig. 6). As already pointed out by Stauffer (1982), NGC 404 is always located near or within the shock-excited region in this diagnostic diagram as well as in others involving, e.g. [O I] 6300 Å. However, photo-ionization models by Ferland & Netzer (1983) span the shock-excited locus in Fig. 6 only by varying the chemical abundance and ionization parameter so that the shock-excitation conclusion is not straightforward if one uses only line ratios in the visible region. On the other hand, the near-infrared lines [S III] 9069, 9532 Å appear to be excellent excitation-mechanism discriminators (Diaz, Pagel & Wilson 1985, hereafter DPW). However, owing to the fact that water vapour absorptions were particularly strong during the observing run, the residues of their correction in our data set are strong and it has only been possible to set upper limits to the [S III] line intensities (Table 6). These upper limits are not stringent enough to identify the excitation mechanism as from shocks (Fig. 7). The line ratios are still consistent with a superposition of a photo-ionization source on a shock-excited plasma. We also show in these diagrams the effect of reddening, which is minor as, even with the strong reddening derived from the line-emitting regions in our objects, the locus of the points or of their upper limits are not significantly displayed in Figs 6 and 7. In Fig. 6, NGC 278 is situated in the region of very low excitation H II regions. In Fig. 7 it sits on a locus not far from the position of H II regions according to DPW and consistent with what is expected from a low excitation H II region. The nucleus of NGC 278 is a site of intense star formation as already denoted through its dominant very young stellar population, and this process seems to be still going on. The low excitation found in this object indicates that most of the H II regions located in the nuclear region are in a late evolutionary stage.

8 CONCLUDING REMARKS

We have observed over the spectral range 3500–10000 Å the blueish nuclear regions of the spiral galaxies M33 and

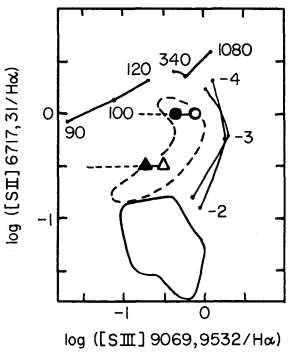

Figure 7. Logarithmic plot of the line-intensity ratios [S II] λλ6717, 6731/Hα versus [S III] λλ9069, 9532/Hα. Theoretical models as in DPW: labels 90 to 1080 stand for the velocities in km s^{-1} sof the shock-wave models; −200 to −400 represent log(U) for photo-ionization models; the continuous line contains H II regions; the dashed line contain DPW's LINERS and NLR Seyfert 1 galaxies. Symbols for NGC 278 and NGC 404 as in Fig. 6. The [S III] intensity values are upper limits.

NGC 278, as well as the nuclear region of the dwarf lenticular galaxy NGC 404. We have applied to these objects a population synthesis method which uses a base of star cluster integrated spectra. The synthesis relies on a grid of star cluster spectral characteristics (equivalent widths and continuum points), as a function of age and metallicity. Whenever necessary we have refined this analysis by using the full spectral information (the point by point star cluster and galaxy spectra). The algorithm used in the first case is a multiple minimization procedure which treats statistically the acceptable solutions, while, in the second case, we have applied a classical minimization procedure.

A simple spectral comparison of the M33 nucleus and globular clusters with $[Z/Z_\odot] \approx -2$ clearly shows drastic spectral differences in the near-infrared, allowing us to reject earlier suggestions of a similar stellar content and of the predominance of an old metal-poor component in M33. Our quantitative synthesis indicates that the early-type spectrum of M33 in the blue arises from young components ($t \leq 5 \times 10^8$ yr) and that the old very metal-poor contribution $[Z/Z_\odot] \leq -1.5$ is negligible. The old population in the range $-1 \leq [Z/Z_\odot] \leq -0.5$ and the intermediate age components are both important. Their relative contribution remains to be determined more precisely from data extending to the ultraviolet spectral range. The metallicity in the nucleus has, at most, reached up to the solar value.

The nucleus of the spiral galaxy NGC 278 is dominated by young components and its emission line spectrum indicates that the star-forming process is still in operation. The maximum metallicity of the stellar population is solar at most. The nucleus of the nearby dwarf lenticular NGC 404 is dominated by an old component with $[Z/Z_\odot] \approx -0.5$. The young component is weaker than in the M33 or NGC 278 nuclei, but it still contributes in a significant way, in particular to the blue flux. The intermediate age component is found to be similar to that derived by Bica (1988) in early-type galaxies. Finally the very metal-poor components provide quite a small contribution in this galaxy.

The emission-line spectra from the gaseous components in these objects were isolated and analysed. In the nucleus of M33 only [N II] 6584 Å has been detected. The emission-line ratios for the NGC 278 nucleus are characteristic of a low-excitation H II region. This suggests that in the crowded nuclear region, the predominant H II regions are in a late evolutionary stage. The emission in the nucleus of NGC 404 is also from low-excitation gas but other mechanisms might be operating, besides photo-ionization by stars.

ACKNOWLEDGMENTS

We thank the staff at the Haute Provence Observatory for assistance during the observations. AS and EB acknowledge a research fellowship from the Brazilian institution CNPq. EB is deeply indebted to the Observatoire de Paris for a three-month financial support.

REFERENCES

Baldwin, J. A., Phillips, M. M. & Terlevich, R., 1981. *Publs astr. Soc. Pacif.*, **93,** 5.
Bica, E., 1988. *Astr. Astrophys.*, **195,** 76.
Bica, E. & Alloin, D., 1986a. *Astr. Astrophys.*, **162,** 21.
Bica, E. & Alloin, D., 1986b. *Astr. Astrophys. Suppl.*, **66,** 171.
Bica, E. & Alloin, D., 1987a. *Astr. Astrophys.*, **186,** 49.
Bica, E. & Alloin, D., 1987b. *Astr. Astrophys. Suppl.*, **70,** 281.
Bica, E. & Alloin, D., 1988. In *Towards Understanding Galaxies at Large Redshifts,* p. 77, eds Kron, R. & Renzini, A., Kluwer, Dordrecht.
Bonatto, C., Bica, E. & Alloin, D., 1989. *Astr. Astrophys.*, **226,** 23.
Burstein, D. & Heiles, C., 1984. *Astrophys. J. Suppl.*, **54,** 33.
Ciani, A., D'Odorico, S. & Benvuti, P., 1984. *Astr. Astrophys.*, **137,** 223.
Cowley, A. P., Crampton, D. & McClure, R. D., 1982. *Astrophys. J.*, **263,** 1.
de Vaucouleurs, G. & de Vaucouleurs, A., 1964. *Reference Catalogue of Bright Galaxies,* University of Texas Press, Austin.
Diaz, A. I., Pagel, B. E. & Wilson, R. G., 1985. *Mon. Not. R. astr. Soc.*, **212,** 737.
Ferland, G. & Netzer, H., 1983. *Astrophys. J.*, **264,** 105.
Gallagher, J. S. Goad, J. W. & Mould, J., 1982. *Astrophys. J.*, **263,** 101.
Keel, W. C., 1983. *Astrophys. J.*, **269,** 466.
McClure, R. D., Cowley, A. P. & Crampton, D., 1980. *Astrophys. J.*, **236,** 112.
Murtagh, B. A. & Saunders, M. A., 1987. *MINOS 5.1 Users Guide,* Technical Report SOL 83-20R, Stanford University, California.
O'Connell, R. W., 1983. *Astrophys. J.*, **267,** 80.
Oke, J. B., 1974. *Astrophys. J. Suppl.*, **27,** 21.
Rubin, V. C. & Ford, W. K. Jr., 1986. *Astrophys. J.*, **305,** L35.
Sandage, A. & Tammann, G., 1981. *A Revised Shapley-Ames Catalog of Bright Galaxies,* Carnegie Institution of Washington.
Schmidt, A. A., Bica, E. & Dottori, H., 1989. *Mon. Not. R. astr. Soc.*, **298,** 925.
Schmidt, A. A., Bica, E. & Alloin, D., 1990. *Astr. Astrophys.*, in press.
Stauffer, J. R., 1982. *Astrophys. J.*, **262,** 66.
Stauffer, J. R., 1983. *Astrophys. J. Suppl.*, **50,** 517.
Stone, R. P., 1977. *Astrophys. J.*, **218,** 767.